Influence of cerium addition and redox state on silicate structure and viscosity

Adrien Donatini, Luiz Pereira, Donald Dingwell, Kai-uwe Hess, Dirk Müller, Laurent Cormier, Daniel Neuville

INFLUENCE OF CERIUM ADDITION AND REDOX STATE ON SILICATE STRUCTURE AND VISCOSITY

Adrien Donatini,[1,2,3*] Luiz Pereira,[4*] Donald B. Dingwell,[4] Kai-Uwe Hess,[4] Dirk Müller,[4] Laurent Cormier,[2] Daniel R. Neuville.[1]

[1] Institut de Physique du Globe de Paris (IPGP), Université Paris-Cité, 75005 Paris, France.

[2] Sorbonne Université, Muséum National d'Histoire Naturelle, CNRS UMR 7590, IRD ERL 206, Institut de Minéralogie, de Physique des Matériaux et de Cosmochimie (IMPMC), 75005 Paris, France.

[3] Corning European Technology Centre, 77212 Avon, France.

[4] Department of Earth and Environmental Sciences, Ludwig-Maximilians-Universität München, 80333 Munich, Germany.

ORCiD (AD): 0000-0002-8187-2470
ORCiD (LP): 0000-0001-9555-0352
ORCiD (DBD): 0000-0002-3332-789X
ORCiD (KUH): 0000-0003-1860-8543
ORCiD (DM): 0000-0002-9681-1056
ORCiD (LC): 0000-0002-3554-0707
ORCiD (DRN): 0000-0002-8487-5001

*Corresponding authors: donatini@ipgp.fr

ABSTRACT

The viscosities of Ce-free and Ce-bearing (~ 1.3 mol%, ~6.5 wt.% Ce_2O_3) soda lime silicate (window glass) melts were measured with respect to oxidation state. Experiments were performed isothermally using a concentric-cylinder viscosimeter on melts equilibrated with successively reducing CO-CO_2 gas mixtures within a gas tight vertical tube furnace at 1 atm. Viscosity measurement and sampling were performed at the end of each melt reduction step. Further, viscosities in the glass transition temperature range were estimated using the shift factor method applied to glass transition temperature values determined using differential scanning calorimetry (DSC) measurements on quenched glasses. The Ce speciation at each stepwise melt reduction was probed using Ce L_3-edge X-ray absorption near-edge structure (XANES) spectroscopy, while structural information upon Ce addition and reduction was provided by Raman spectroscopy. The viscosities of these materials remain constant at this level of Ce addition and do not vary significantly with redox state at high temperature. Conversely, viscosity values in the glass transition temperature range increase upon both Ce addition and reduction. Our analysis, based on the glass composition analyses obtained via electron probe micro-analyzer (EPMA), viscosity calculations, and observations of silicate structural changes, leads to the conclusion that the observed viscosity increase around the glass transition temperature is explained by the high ionic field strength of Ce ions as well as the polymerization behavior of the silicate matrix occurring during reduction of Ce. Because of its low concentration, resulting from its low solubility, Ce redox changes exert only minimal effects on the viscosity of this melt.

Keywords: glass, redox, differential scanning calorimetry, XANES spectroscopy, Raman spectroscopy.

1. INTRODUCTION

Rare-Earth elements (REEs) are of extreme importance in both geosciences and material sciences.[1, 2] Among these elements, Ce, when present in oxide glasses and melt under terrestrial conditions, can exist in two distinct redox states, i.e., Ce^{3+} and Ce^{4+}. The Ce speciation, as for other multivalent elements like iron, is a function of several factors such as total Ce content, oxygen fugacity, glass composition, and temperature.[3–5] Ce doped glasses are attractive materials for a wide range of research activities. In geoscience, Ce distribution between coexisting phases (i.e., mineral/melt) may be used as an indicator for the genetic history of magmatic liquids.[1] In optical devices, Ce has been largely used due to its efficacy in blocking ultraviolet radiation.[6] In the context of nuclear waste vitrification, Ce is generally a fission product found in high-level waste.[5, 7] Moreover, the presence of this element, along with its redox state, can exert influence on the formation and behavior of bubbles[8, 9]. These bubbles, in turn, influence the electrical response of these systems, thereby regulating the high-temperature processes and influencing the quality of the final product.[10]

Ce speciation (e.g., Ce^{+3}/Ce_{tot}) in glasses is known to play a crucial role, modulating various spectroscopical and physical properties of Ce-bearing systems.[6, 11] For instance, Ce plays a significant role on characteristic glass temperatures, including glass transition temperature and onset crystallization.[11] Past studies have shown that the introduction of Ce into the glassy network induce an increase of the glass transition temperature for silicate systems, a similar observation was made upon cerium reduction[11, 12]. This indicates a strengthening of the glassy network upon Ce introduction and reduction.

The viscosity of silicate liquids plays an important role in determining the time-scale of several phenomena taking place in silicate melts at relatively high temperature, encompassing crystal growth, mass transfer, bubble behavior, and crystal aggregation.[13–16] As a result, liquid viscosity stands out as one of the most pivotal physical properties during high temperature processes in both natural and industrial contexts. Viscosity of melts containing multivalent elements is known to be influenced by the speciation of these elements. Studies have shown that the iron reduction in silicate melts promotes a non-linear viscosity decrease, with a higher dependency on redox in oxidized regions.[17–19] Interestingly, contrary to expectations within the silicate melt community, Casas et al.[20] observed that iron reduction in molten pyrolite (Fe-bearing silicate) promotes small viscosity increases, consistent with the polymerization behavior of their studied system. In addition to iron, cerium can also influence the viscosity of silicate melts[21–23]. It has been shown that the addition of Ce reduces the viscosity of a simplified silicate melt composition through the depolymerization of the silicate network[21]. However, there is a notable gap in the literature regarding the viscosity of Ce-bearing melts, particularly concerning the effect of Ce oxidation or reduction on viscosity of silicate melts. Addressing this gap is crucial for advancing our understanding of the role of cerium in modifying the rheological properties of silicate materials.

In this current work, we investigate the viscosity of both Ce-free and Ce-bearing window glasses at the glass transition temperature range as well as at high temperature. We performed the experiments for varying redox

states for the Ce-bearing samples. In this studied case, Ce is the only multivalent element and no redox coupling has been introduced. Here, we varied the Ce redox state using different gas mixtures in a vertical gas tight tube furnace during viscosity measurement. The glasses were sampled at the end of each melt reduction step and characterized using Raman and XANES spectroscopies. In this article, using these high-temperature experiments together with structural information and Ce speciation, we aim to shed light on the effect of Ce addition and redox state on the viscosity of window glass.

2. MATERIALS AND METHODS

2.1) Glass synthesis

The starting materials were obtained by mixing a window glass powder with 1.3 mol% (i.e., ~6.5 wt.%) of Ce_2O_3 as CeO_2 powder. The window glass is the same as used in Wadsworth et al.[24] and the CeO_2 powder is from ChemPUR (chemical purity 99.99%). These powders were homogenized and about 100 g of this mixture was melted under air in a Pt_{80}-Rh_{20} thick-walled viscometry crucible. We synthesized this mixture above 1200 °C during approximately 12 h at 1 atm and in air in a furnace coupled with a concentric cylinder apparatus. This setup facilitated effective removal of bubbles and ensured compositional homogenization.

2.2) Electron probe micro-analyzer

Chemical compositions were determined using a Cameca SX100 electron microprobe. The analytical conditions were set at 15 kV, 5 nA, and a defocused beam of 10 µm in order to prevent alkali migration. The following standards were used for calibration: Si, Na - albite; K, Al - orthoclase; Ca - wollastonite; Mg - periclase; Fe - syn. Fe_2O_3; Ce - syn. $CePO_4$. Counting times of 10 s on the peak and 5 s on each background (left and right side of the peak) were applied for Na, Si, Al, Ca, Mg, and Ce. For K the counting time was 10 s on peak and background, while it was extended to 30 s for Fe. To further decrease detection limit for Fe, simultaneous measurements on two spectrometers were conducted, with results averaged afterward. The values displayed in Table 1 is the average composition of at least 20 analyzed points for each of the glasses.

Table 1: Normalized chemical composition of the Ce-free glass and Ce-bearing glasses (in wt.%) obtained via EPMA (standard deviations are given in parenthesis and the measured totals are given in brackets). The relative error is of ± 5% for concentrations for values < 10 wt% and ± 1.5 % for values > 10 wt.%.

Oxides	*Ce-free*	*WG 1.3 Ce-a*	*WG 1.3 Ce-b*	*WG 1.3 Ce-c*	*Detection limit (d.l.)*
SiO_2	72.48 (0.73)	67.88 (0.48)	68.26 (0.65)	69.46 (0.63)	0.14
Al_2O_3	0.60 (0.04)	0.54 (0.04)	0.55 (0.05)	0.55 (0.05)	0.09
$Fe_2O_3^{tot}$	< d.l.	< d.l.	< d.l.	< d.l.	0.08
MgO	3.86 (0.09)	3.61 (0.07)	3.67 (0.11)	3.53 (0.10)	0.08
CaO	9.35 (0.11)	8.69 (0.15)	8.53 (0.18)	7.76 (0.12)	0.09

Na_2O	13.49 (0.47)	12.42 (0.56)	12.43 (0.28)	12.04 (0.28)	0.17
K_2O	0.22 (0.04)	0.23 (0.03)	0.19 (0.04)	0.22 (0.03)	0.06
$Ce_2O_3^{tot}$	< d.l.	6.63 (0.11)	6.37 (0.23)	6.44 (0.19)	0.30
Total	100 [99.95]	100 [99.57]	100 [99.97]	100 [99.96]	-

2.3) Viscosity at high-temperature range

The viscosity measurements at 1199 °C were acquired at the Ludwig-Maximilians-Universität München (Munich, Germany) using a concentric-cylinder technique in a vertical alumina muffle tube furnace equipped with a CO/CO_2 gas mixture line.[18] The top of the furnace was adapted with an iris diaphragm that allows the spindle to pass through. The ambient oxygen fugacity in the furnace was fixed by controlling the furnace atmosphere using air, pure CO_2, and successively reducing CO/CO_2 mixing ratios (cf. Table 2). These gas mixtures give rise to different oxygen fugacities which were continuously monitored using a solid state oxygen fugacity electrode and a voltage meter. The oxygen fugacity values were calculated using $\log(fO_2) = 0.679 + 20.16\left[\frac{V}{T}\right]$ where fO_2 is the oxygen fugacity, V is the voltage in mV, and T is the temperature in Kelvin.[17] More information on viscosity measurements and the redox conditions of the system can be found in Table 2. The glass, together with the Pt_{80}-Rh_{20} thick-walled viscometry crucible, was introduced in this experimental set-up. After approximately 1 h of thermal and mechanical stabilizations, viscosity measurements were initiated using a Brookfield rheometer head model RVTD III. Additional details about the setup can be found elsewhere.[17, 25] To achieve thermodynamic equilibrium with the next imposed gas mixture, the melts were equilibrated in the furnace for at least 6 days. The sampling procedure for subsequent characterizations (i.e., Raman spectroscopy, DSC, EPMA, and XANES spectroscopy) was carried out at the end of each stepwise melt reduction by inserting an alumina stick and collecting a few hundred milligrams of glass that had been quenched in water using the dip quench technique. This approach aimed to be as fast as possible to avoid any re-oxidation of the melt during the sampling procedure. The reduction of the collected glasses was confirmed using XANES spectroscopy measurements. These quench rates are enough to block the Ce oxidation state from high-temperature scenarios in the glassy material.

Table 2: Studied glass samples along with their experimental conditions in the high-temperature concentric cylinder viscometer coupled with gas mixing of CO/CO_2. Numbers in the parentheses for the atmosphere column represents the CO and CO_2 gas fluxes in cm^3/min.

Sample	*Atmosphere*	*Voltage (mV)*	*log(fo_2, atm)*	*Temperature (°C)*
Ce-free	Air	3.2	-0.723	1199
WG 1.3 Ce-a	Air	3.2	-0.723	1199
WG 1.3 Ce-b	CO_2 (20)	490.0	-2.870	1199
WG 1.3 Ce-c	CO/CO_2 (16/4)	690.8	-10.133	1199

2.4) Viscosity at T_g temperature range

Calorimetry has been suggested as a method to retrieve indirectly the viscosity of glasses in the vicinity of their glass transition temperature (T_g).[26] The equivalence of enthalpic and shear stress relaxation times implies the applicability of a simple equation (Eq. 1) to combine both shear viscosity and cooling rate in order to predict the viscosity at the glass transition temperature using a constant shift factor K for a given glass composition:[26]

$$\log_{10}(\eta_{\text{at Tg}}) = \text{K} - \log_{10}(|q_{c,h}|), \quad (1)$$

where $\eta_{\text{at Tg}}$ is the viscosity of the material at the glass transition temperature, $q_{c,h}$ is the cooling and heating rates used during DSC measurements, and K is the shift factor which is a function of the glass composition.[27] To derive the shift factor for our current system, we used the 'excess oxide' approach presented in Gottsmann et al.[27] The excess oxide, for the current system, is calculated by subtracting the sum of the molar percentages of Al_2O_3 (considered as a structural network former), from the sum of the molar percentage of oxides considered as network modifiers (MgO, CaO, Na_2O, K_2O, and Ce_2O_3). Here, we considered that Ce_2O_3 plays a network modifier role in the silicate network. This assumption has a negligeable impact on the obtained results since our current system is already depolymerized and, as such, is not highly sensitive to the excess oxide value (see Gottsmann et al. for more details).[27] Using the obtained values of excess oxide for each of the studied samples, one can obtain the shift factor value using Eq. 2:[27]

$$\text{K} = 10.321 - 0.175 \ln(x), \quad (2)$$

where x is the excess oxide value in mol%. As shown in Gottsmann et al.[27] and mentioned in the previous paragraph, the excess oxide value becomes less dependent on the composition for depolymerized glasses, such as the current studied window glass composition. Consequently, the reduction of Ce and a possible change in its structural role in the glassy network would have little effect on the excess oxide value. By applying this method for the studied compositions, the values of excess oxide and the corresponding shift factor could be retrieved.

Subsequently, we determined the glass transition temperature (defined as the peak temperature) required to achieve the viscosity of the material at this specific temperature. Hence, DSC measurements were executed using a Netzsch STA 449 F1 and using about 30 mg of glass (which was conditioned with a cooling rate of 10 °C min^{-1}) at heating rate of 10 °C min^{-1} under an Argon atmosphere. A temperature calibration has been done using the melting points of In, Al and Au; the absolute error of the measurement is ± 2 °C.

2.5) Ce L_3-edge X-ray absorption near-edge structure

Ce L_3-edge XANES spectra were recorded on the LUCIA beamline at the SOLEIL synchrotron facility (Saint-Aubin, France) operating at 2.72 GeV and 500 mA. XAS spectra were collected in fluorescence mode using a SDD detector.[28] A Si(111) double crystal monochromator was used for the incoming X-ray calibrated at the first inflexion point of the Ti K-edge (4966 eV) using a Ti foil. A macro beam of 3 × 3 mm was used in order to minimize photo-oxidation of the samples. Spectra were acquired in continuous mode (FLYSCAN) from 5680 eV to 5850 eV with a 0.2 eV resolution and 300 ms per step. At least 3 scans were collected on all samples to study their photo-oxidation. The XANES data obtained were processed using the Larch software.[29] Linear functions were used for both pre-edge and post-edge fitting. A linear combination of endmembers was performed in order to determine Ce redox states, see section 3.2 for details.

2.6) Raman spectroscopy

Unpolarized Raman spectra were acquired using a Labram HR Evolution spectrometer equipped with a Peltier-cooled CCD and an 1800 lines per mm grating. The samples were excited with a Coherent MX 488 nm solid-state laser focused through a × 50 Olympus objective on the sample surface. The spectral resolution of the setup is ~1.7 cm^{-1} and the spatial resolution is ~1 µm. The laser power was adjusted to 600 mW. Spectra were acquired from 20 to 1500 cm^{-1} thank to an ULF filter to attenuate laser signal. A linear baseline was fitted over the 1350-1500 cm^{-1} range. Spectra fitting was performed using the Fityk software with the Levenberg-Marquardt method.[30]

3. RESULTS

3.1. Viscosity results of Ce-free and Ce-bearing window glasses

Figure 1 illustrates the viscosity evolution of a Ce-bearing melt, denoted WG 1.3 Ce-b, (cf. Table 1 and Table 2), from the beginning of the experiment, following the setting of the new gas composition, until thermal and mechanical stabilizations. One can observe that the viscosity remains constant, within the measurement error, along the whole experimental duration. No discernible viscosity change is observed during the redox re-equilibration with the new atmosphere at this relatively high-temperature region (i.e., ~1200 °C). It is important to emphasize that the viscosity values do not change significantly beyond the experimental error range (± 0.02 log units). This observation is consistent across other samples analyzed under different redox conditions, where both initial and final results demonstrate a similar consistency.

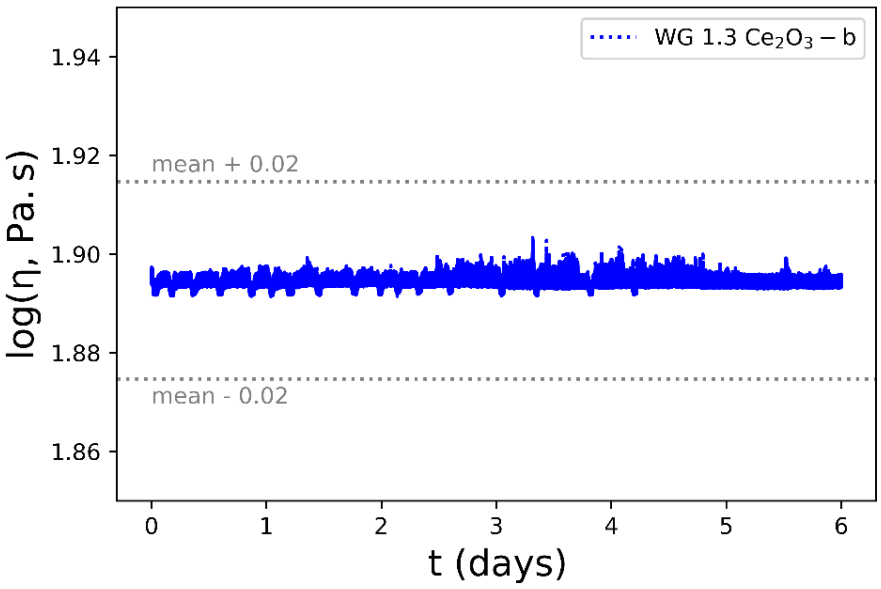

Figure 1: Viscosity evolution for the sample WG 1.3 Ce2O3 - b measured at ~1200 °C showing that during the redox change over ca. 6 days the viscosity remains relatively constant and the values are within the error of the measurement confirming the absence of significant viscosity change.

The other samples, evaluated at different redox ratios, also presented identical initial and final values of viscosity within the experimental error of 0.02 log units, similarly to what is observed in Figure 1. Table 3 summarizes the viscosity at the end of each reduction stepwise after redox equilibration with the controlled atmospheres. Table 3 displays the viscosity of the Ce-free and Ce-bearing samples at different redox conditions measured at 1199 °C along with the relative errors on viscosity. The equilibrium values are equal within the experimental error. Consequently, the addition or reduction of Ce in the molten glass exerts negligible influence on the viscosity of window glass melts at relatively high temperature scenarios (i.e., ~1200 °C).

Table 3: Viscosity results obtained using a concentric-cylinder viscometer on melts equilibrated with air, CO_2, and CO/CO_2 gas mixtures in a vertical tube (gas-mixing furnace). The viscosity values were obtained after redox equilibration at ~1200 °C.

Sample	$log_{10}(\eta; Pa.s)$ *at high-T*	$log_{10}(error; Pa.s)$ *at high-T*	*Temperature (°C)*
Ce-free	1.88	± 0.02	1199
WG 1.3 Ce_2O_3 - a	1.90	± 0.02	1199
WG 1.3 Ce_2O_3 - b	1.89	± 0.02	1199
WG 1.3 Ce_2O_3 - c	1.89	± 0.02	1199

To retrieve the viscosity in the glass transition temperature range, we used the shift factor along with the glass transition temperature obtained via DSC measurements (cf. section 2.3). Figure 2 shows the DSC curves for the four studied samples displaying the glass transition temperature for each of these materials. It can be observed a relatively strong T_g increase upon Ce addition and also a slight T_g increase upon Ce reduction. It is important to stress that the experimental error in this case is ± 2 °C and therefore these T_g values, displayed

in Figure 2, fall outside the error margin of the measurements. Table 4 displays the excess oxide, shift factor, glass transition temperature, and the final calculated viscosity at the DSC glass transition temperature using the previously mentioned parameters and corresponding equations.

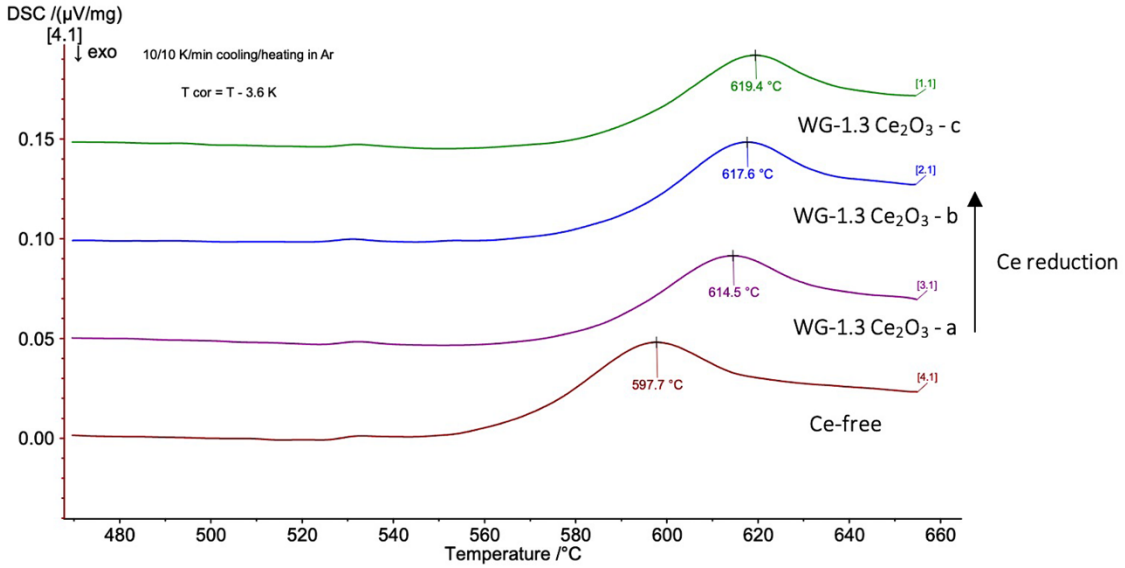

Figure 2: Differential scanning calorimetry results on Ce-free and Ce-bearing materials measured under argon atmosphere. The glass transition temperatures are pointed out in the figure and the temperature correction is annotated on the figure. The absolute error in the glass transition temperature measurements is equal to ± 2 °C. For better visibility, the heat flow curves (y-axis) were shifted by 0.05 mV/mg.

Table 4: Excess oxide, shift factor, glass transition temperature and viscosity at T_g.

Sample	*Excess oxide (mol%)*	*Shift factor, K*	*Glass transition temperature, T_g (°C)*	$log_{10}(\eta_{at\ Tg}; Pa.s)$
Ce-free	28.07	9.74	594 ± 2	10.52 ± 0.1
WG 1.3 Ce_2O_3 - a	27.82	9.74	611 ± 2	10.52 ± 0.1
WG 1.3 Ce_2O_3 - b	27.56	9.74	614 ± 2	10.52 ± 0.1
WG 1.3 Ce_2O_3 - c	25.51	9.75	616 ± 2	10.53 ± 0.1

It is known that multivalent speciation is not only a function of oxygen fugacity (fo_2), but is also temperature-dependent.[3–5] Since the Ce-free sample does not contain multivalent cations, it was possible to measure its viscosity for various temperature and attribute the evolution of viscosity to the temperature change only and not to a potential change in redox state. These high-temperature measurements were obtained from ca.1200 – 1000 °C and will be presented later in this section. Therefore, in order to obtain more information on these systems, we consider that at high temperature (i.e., ~ 1000 – 1200 °C), the viscosity of all samples do not significantly vary from that of the Ce-free sample. This simplification, coupled with the individual values of viscosity in the low-temperature range obtained via DSC data and shift factor calculations (Table 4), allow us to determine the Vogel–Fulcher–Tammann (VFT) parameters and fragility for these silicates. The experimental viscosity values were fitted using the (VFT)[31–33] equation to describe the temperature dependence of these viscosities (Eq. 3):

$$\log_{10}(\eta_{liquid}) = A_{VFT} + \frac{B_{VFT}}{T - C_{VFT}}, \quad (3)$$

where A_{VFT}, B_{VFT}, and C_{VFT} are the fitting parameters of the VFT equation. To determine the fragility of these glasses, we first calculate the 'Angell' glass transition temperature value ($T_{g12\ VFT}$), which is defined as the temperature at which the viscosity value equals 10^{12} Pa.s (Eq. 4). The fragility can be understood as the degree to which the temperature dependence of the viscosity deviates from an Arrhenian behavior and is expressed in terms of the kinetic fragility index (m_{VFT}) (Eq. 5).[34] Fragile materials possesses high m_{VFT} indexes, while strong materials have small index values. In Table 5, we reported the fitting parameters A_{VFT}, B_{VFT}, and C_{VFT}, together with $T_{g12\ VFT}$ and m_{VFT} calculated with the following equations:

$$T_{g12\ VFT} = C_{VFT} + \frac{B_{VFT}}{12 - A_{VFT}}, \quad (4)$$

$$m_{VFT} = \frac{B_{VFT}}{T_{g12\ VFT}\left(1 - \frac{C_{VFT}}{T_{g12\ VFT}}\right)^2}. \quad (5)$$

Table 5: VFT coefficients and kinetic fragility index for the investigated samples obtained using Eq. (4) and Eq. (5) from the experimental viscosity data measured at relatively high- and low-temperature regions.

Sample	A_{VFT}	B_{VFT}	C_{VFT}	$T_{g12\ VFT}$	m_{VFT}
	$log_{10}(\eta; Pa.s)$	K	K	K	-
Ce-free	-2.23 ± 0.03	3675 ± 33	579.02 ± 2	837	46
WG 1.3 Ce_2O_3 - a	-1.95 ± 0.05	3257 ± 51	622.71 ± 3	856	51
WG 1.3 Ce_2O_3 - b	-1.93 ± 0.04	3215 ± 41	628.83 ± 3	859	52
WG 1.3 Ce_2O_3 - c	-1.92 ± 0.04	3194 ± 38	632.46 ± 2	861	52

We compiled the viscosity obtained at both high- and low-temperature scenarios along with the VFT fitting curves in Figure 3. As shown, the effect of Ce addition and its reduction is more pronounced for viscosity at low temperatures compared to relatively high temperatures.

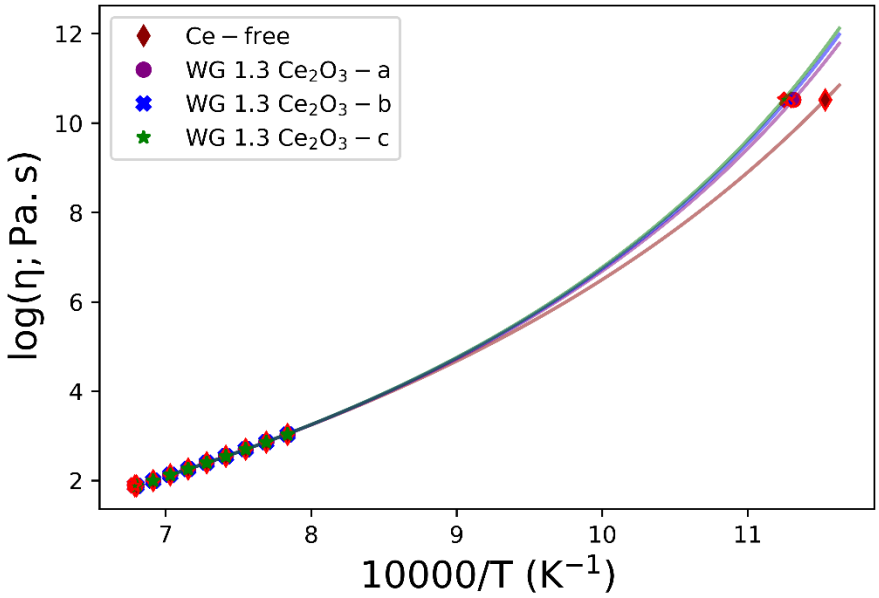

Figure 3: Viscosity as a function of the reciprocal of temperature in the whole measurable temperature range. The experimental obtained values at both relatively high and low temperatures (i.e., viscosity at the glass transition temperature and viscosity at 1199 °C) were highlighted with a red marker color edge. The values at high temperatures (ca. 1000 – 1200 °C) were taken to be equal to the viscosity values obtained for the Ce-free sample and are displayed without marker color edge. Errors are smaller than the symbol size. The continuous lines are the VFT fits for the values displayed as symbols.

3.2. XANES spectroscopy results

To confirm the reduction of Ce during the high-temperature viscosity experiments under a controlled atmosphere, we performed XANES spectroscopy measurements. Figure 4 displays the XANES spectra for monazite ($CePO_4$) and Ce oxide (CeO_2) which are used as references for Ce^{3+} and Ce^{4+}, respectively. The three studied samples containing Ce are also included in this figure. The XANES spectrum of WG 1.3 Ce_2O_3 - c sample, which is the most reduced one, is very close to that of the crystalline monazite reference (Figure 4.A). The deviation can be attributed to differences in the local environment of Ce rather than a distinct redox state, this is especially true concerning the first EXAFS oscillation. This observation qualitatively indicates the Ce^{3+} local structure is different in our glass than in monazite. The Ce redox state, here evaluated as Ce^{3+}/Ce_{tot}, can be determined by linear combinations. The use of crystalline CeO_2 as an endmember leads to a deviation in the fit around 5735 eV (see supplementary Figure S1). This discrepancy is attributed to the structuration of the L_3-edge, namely the sharp peaks visible in Figure 4.A at 5731.5 and 5738.5 eV. However, due to the high redox potential and the very low solubility of Ce^{4+} in silicate glasses,[35, 36] it is difficult to obtain fully oxidized Ce in our system. Therefore, we opted for choosing a crystalline reference rather than a partially oxidized glass as endmember. Table 6 shows the obtained redox ratio for the WG 1.3 Ce_2O_3 series, determined by linear combinations using the sample 'WG 1.3 Ce_2O_3 - c' as the reduced endmember and crystalline CeO_2 as the oxidized one. The measured redox states were then compared to the model developed by Pinet et al.[5] to predict Ce redox equilibrium at high temperatures and the results of the comparison are presented in Figure 5 as well as Table 6.

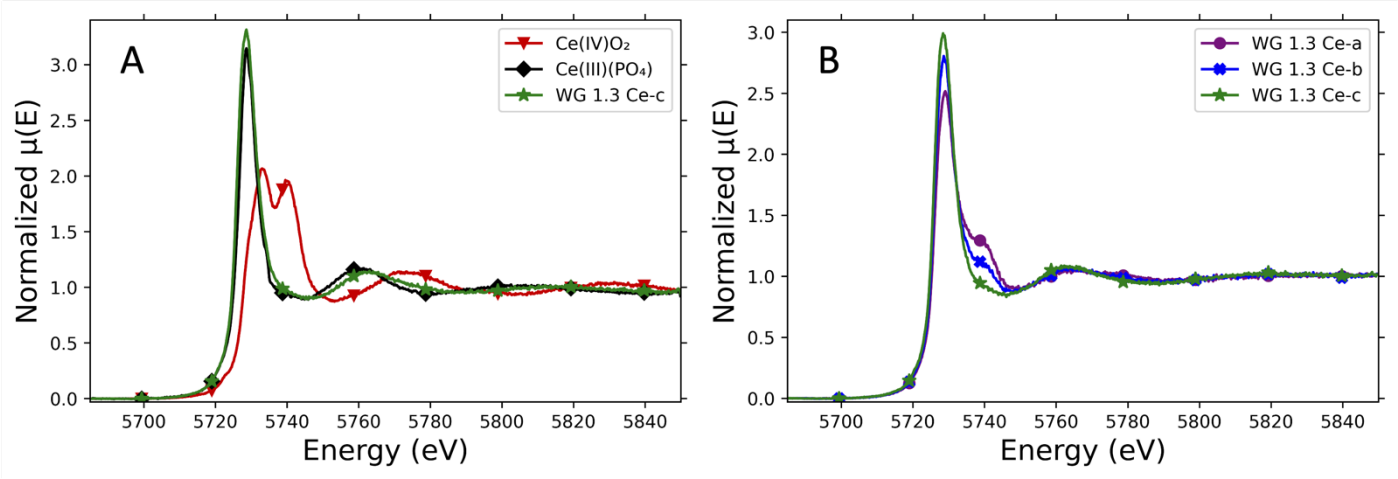

Figure 4: XANES spectra of the two reference materials as well as the three Ce-bearing glasses at different redox conditions.

Table 6: Information extracted from the XANES spectra along with quantification of Ce speciation in the glass. The measured Tg values from table 4 are also reported.

Sample	*log(fo_2, atm)*	Ce^{3+}/Ce_{tot}(%) XANES	Ce^{3+}/Ce_{tot}(%) *Pinet et al. model*	*Measured Tg (°C)*
Ce-free	-0.723	-	-	594 ± 2
WG 1.3 Ce_2O_3 - a	-0.723	67 ± 3	61 ± 5	611 ± 2
WG 1.3 Ce_2O_3 - b	-2.870	84 ± 3	85 ± 5	614 ± 2
WG 1.3 Ce_2O_3 - c	-10.133	100 ± 3	100 ± 5	616 ± 2

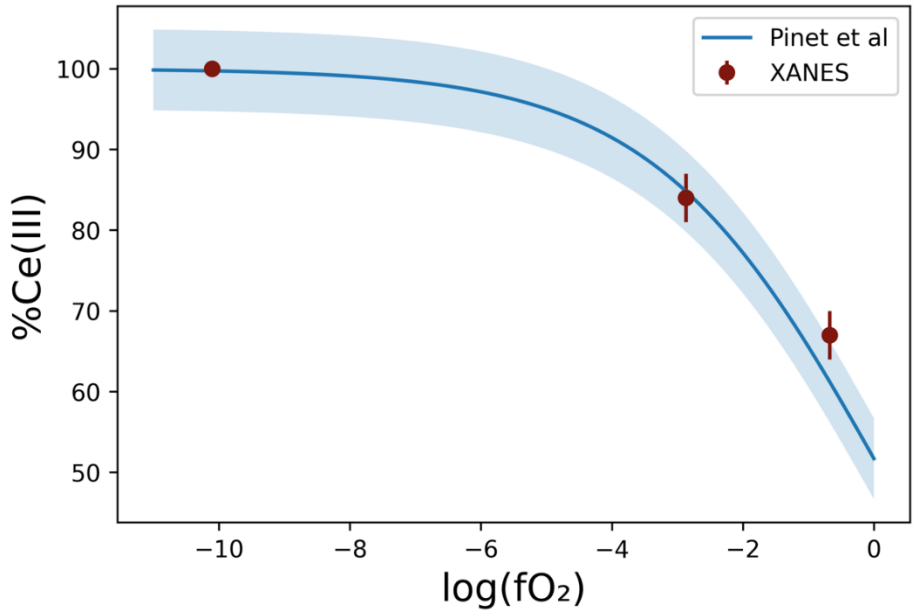

Figure 5: Comparison between the redox state of the samples quenched from 1200°C under different atmospheres measured by XANES spectroscopy at room temperature and the values predicted by the model of Pinet et al at 1200°C under different atmospheres.

The redox ratios obtained at room temperature are in accordance with the ones predicted at equilibrium at high temperature. This shows that the samples are at thermodynamic equilibrium, which was expected given the high dwelling time and the stirring provided in the viscometer. More importantly, it shows that the sampling and quenching were performed successfully, retaining the high temperature redox state. This was shown in a previous study performed on a sodium aluminosilicate glass quenched from 1600°C.[37]

3.3 Raman spectroscopy results

To elucidate the structural changes associated with both Ce addition and reduction, Raman spectroscopy measurements were carried out on the Ce-free and Ce-bearing glasses. Figure 6 shows the spectra of these materials. Upon addition of Ce, significant changes occur in the 750-1350 cm^{-1} region of the Raman spectra, which are related to the vibrations of the TO_4 tetrahedron (with T = Si, Al).[38] The intensity of the boson peak, at low wavenumbers, increases significantly upon Ce addition (Figure 6.A). Upon Ce reduction, the intensity of the boson peak diminishes but, even when Ce is fully reduced (WG 1.3 Ce-c), the boson peak is still more intense than in the Ce-free glass. However, this evolution will not be further discussed here. The region of interest for the study is the 750-1350 cm^{-1} region, as displayed in Figure 6.B. Compared with Ce-free glass, the spectra of Ce-doped glasses are slightly shifted towards lower wavenumbers. The appearance of a new contribution upon Ce addition is also perceptible between 900 and 1000 cm^{-1}.

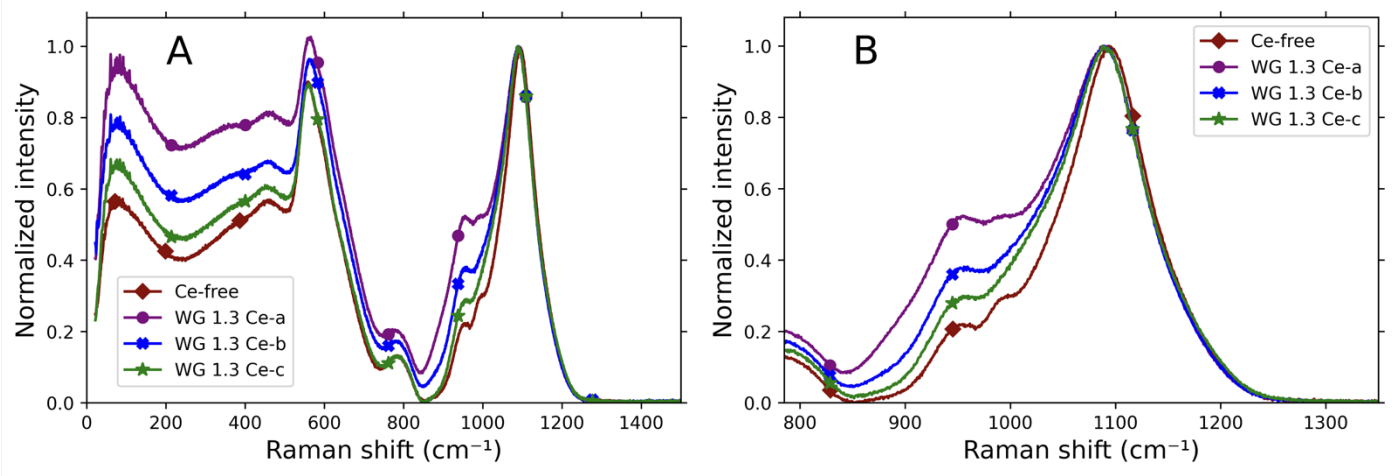

Figure 6: A) Raman spectra of Ce-free and Ce-bearing glasses equilibrated at various redox ratios and B) highlighted area of interest to understand the impact of both Ce addition and reduction on the glass structure.

Here, a simple linear background was fitted over the 1350-1500 cm^{-1} region before performing the decomposition of the spectra. An additional Gaussian background was fitted at low wavenumbers, its position was set to 786 cm^{-1}. The evolution of this contribution will not be discussed further, as it is only used to isolate the region of interest from the rest of the spectra. The decomposition of the Ce-free glass, shown in figure 6A, uses five Gaussian functions named therein. Vibrations labelled Q^2, $Q^{3(I)}$, $Q^{3(II)}$, and Q^4 correspond to symmetric A_1 vibrations of a SiO_4^{4-} tetrahedron, with the notation Q^n corresponding to 'n' bridging oxygen (BO). The use of two different Q^3 vibrations, labelled $Q^{3(I)}$ and $Q^{3(II)}$, will be discussed in the following paragraphs. The vibration labelled T_{2S} is an asymmetric stretching T_2 vibration of the SiO_4^{4-} tetrahedron.[38–41]

Figure 7 displays the Raman spectrum for the Ce-free glass along with those for the Ce containing glasses for various redox conditions. It includes the individual contributions of each vibration, in addition to the background, sum, and residuals.

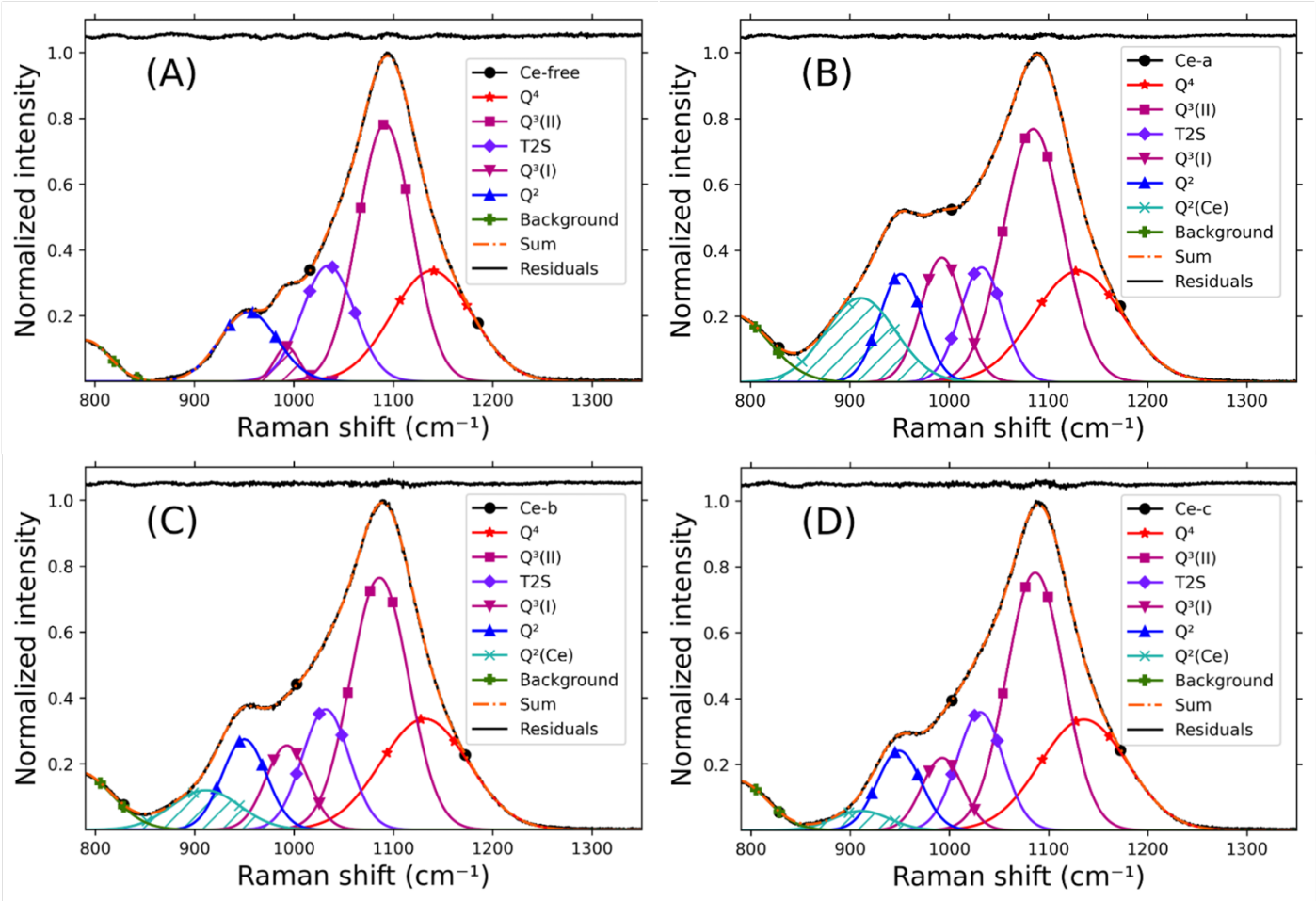

Figure 7: Raman spectra for the Ce-free sample (A) together with the Ce-bearing glasses under increasingly reducing conditions from (B) to (D). Additionally, the deconvolution of the overall spectra includes the sum of these contributions, as well as the residuals. Q^3

The shoulder visible at around 980 cm^{-1} imposes the use of an additional band beyond the four expected ones. We interpret this vibration as a second type of Q^3 units, potentially due to the presence of several cations in the glass that could compensate the NBO charge, namely Na and Ca ions and non-negligible amounts of Mg.[42] We label those two types of Q^3 units: $Q^{3(I)}$ and $Q^{3(II)}$. However, no second Q^2 contribution can be reliably isolated from the present decomposition (Figure 7). On the other hand, the Q^2 contribution in this studied case is relatively large (approximately 34 cm^{-1}), this can suggest multiple Q^2 environments that are too similar to be properly isolated in the decomposition.

Upon addition of Ce, a supplementary contribution is required to adequately fit the spectra. We attribute this vibration, centered at 911 cm^{-1}, to a new type of Q^2 units, at least partially compensated by Ce ions, and hence named $Q^{2(Ce)}$. Both trivalent and tetravalent Ce have higher cationic field strength (CFS: Ce^{3+}= 0.53 $Å^{-2}$; Ce^{4+}= 0.79 $Å^{-2}$) than Na (0.19 $Å^{-2}$), Ca (0.33 $Å^{-2}$), and Mg (0.46 $Å^{-2}$) ions.[43] Therefore, this can explain why the $Q^{2(Ce)}$ band has a smaller Raman shift compared to the regular Q^2 band.[44, 45]

Noteworthily, the relative area of the $Q^{3(I)}$ band increases greatly upon addition of Ce. Although this could be due to a shift from $Q^{3(II)}$ to $Q^{3(I)}$ upon addition of Ce oxide, the most reasonable explanation is the formation of new $Q^{3(Ce)}$ units, similar to the $Q^{2(Ce)}$ one.[46,47] This $Q^{3(Ce)}$ vibration overlaps with the already existing $Q^{3(I)}$ unit, making them appear as a single Gaussian in the decomposition. A similar observation was made in a sodium aluminosilicate glass where the $Q^{2(Ce)}$ band was isolated in the decomposition but not the $Q^{3(Ce)}$ one.[37] All vibrations that were already present in the Ce-free glass are shifted towards lower wavenumbers upon Ce addition. Q^4 shifts from being centered at 1139 cm^{-1} to 1129 cm^{-1}, while $Q^{3(II)}$ center shifts from 1092 cm^{-1} to 1084 cm^{-1}. This can be explained by the addition of a heavy ion in the glass network, therefore shifting the vibrations towards lower wavenumbers.

4. DISCUSSION

We observed a small compositional change, possibly involving the volatilization of alkalis, for the samples quenched after the high-temperature viscosity measurements (cf. Table 1). Two main hypotheses are discussed to explain the observed viscosity changes upon Ce addition and reduction: (i) the compositional changes due to a possible volatilization of elements at high-temperature experiments, leading to silica enrichment, or (ii) the Ce behavior itself in the silicate network during its addition and reduction.

4.1) Are silicate compositional changes controlling viscosity?

To determine if the compositional variations linked to the minor volatilization of alkali and alkaline earth elements during the high-temperature experiments were the controlling factor dictating the observed viscosity changes, we calculate the viscosity of these glasses without considering the presence of Ce oxide. For this purpose, we used the multitask deep neural network model 'GlassNet' developed by Cassar.[48] This neural network model is well suited for the study of such Ce-free base glasses, i.e. window glasses.[48] We chose not to use models and neural networks designed for natural silicate melts, as our compositions fall outside their compositional range.[49–52]

To evaluate the effect of the isolated remaining glass matrix (i.e., in the absence of Ce), we studied the Ce-free base compositions according to the EPMA measurements presented in Table 1. The viscosities calculated using the 'GlassNet' neural network showed only a minor variation in viscosity. However, the calculated changes were much smaller than the ones experimentally observed. Table 7 displays both the viscosity at 587°C obtained using the VFT fit of the experimental data (see Table 5), as well as the viscosity values predicted using neural network on the Ce-free base glass. For this relatively low-temperature scenario, the real viscosity variation observed through the VFT fit of the experimental data presents a much stronger viscosity change when compared to the Ce-free base glasses calculated using neural network. It is important to emphasize that what is relevant here is the relative variation and not the absolute variation. Figure 8 shows the viscosity calculated using neural network as a function of the reciprocal of temperature. For the entire

temperature range, the small compositional variations of the remaining silicate matrix, discounting the Ce effect, are not sufficient to justify the viscosity changes observed experimentally.

Table 7: Viscosity of supercooled window glasses at T = 587 °C determined using (i) VFT fit of the experimental data (cf. Figure 3) and (ii) the 'GlassNet' neural network. The samples used by the neural network are the Ce-free base samples.

Samples	$log_{10}(\eta; Pa.s)$	$log_{10}(\eta; Pa.s)$
	VFT (Experimental)	*Cassar 2023 (Ce-free base sample)*
Ce-free	10.85	10.50
WG 1.3 Ce_2O_3 – a	11.78	10.53
WG 1.3 Ce_2O_3 – b	11.98	10.52
WG 1.3 Ce_2O_3 – c	12.12	10.49

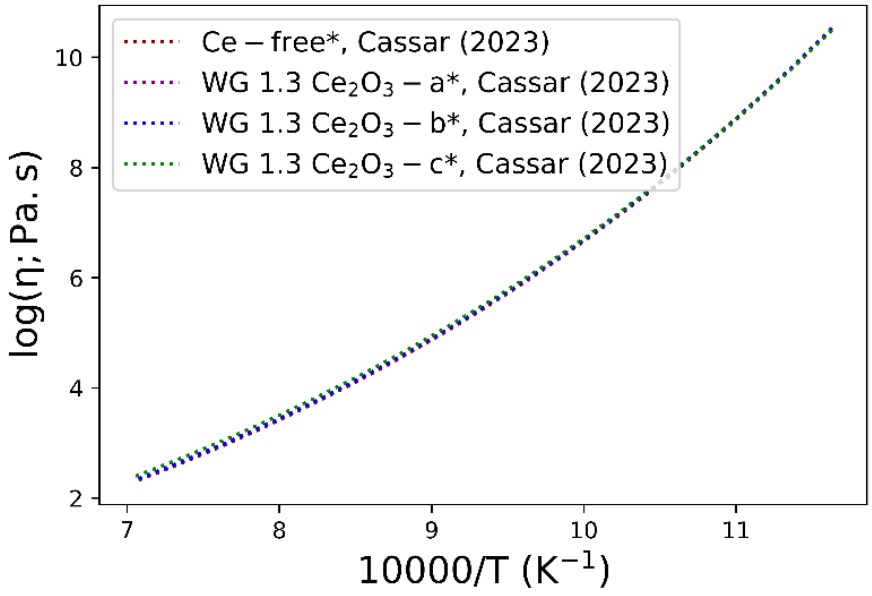

Figure 8: Viscosity of glasses discounting the Ce presence (i.e., compositions were calculated in the Ce-free base glass) as a function of the reciprocal of temperature in the whole measurable temperature range estimated using the 'GlassNet' neural network. In the entire temperature range, similar viscosity values are observed for all the glasses, regardless of a potential volatilization of alkali and alkali-earth elements.

Therefore, based on the viscosity calculations using both 'GlassNet' and the VFT fit of the experimental data, one can conclude that the experimental viscosity variations observed during both the addition and reduction of Ce are not related to volatilization of elements during the high-temperature viscosity experiments and hence are not related to small compositional changes. Instead, these variations may be attributed to the Ce structural role in silicate melts as well as its redox speciation.

4.2) Ce incorporation and reduction in silicates and impact on structure and viscosity

At high-temperature conditions (i.e., ~1200 °C), the viscosities of the Ce-free and Ce-bearing melts are equal upon both Ce addition and Ce reduction (cf. Table 3 and Figure 3). However, at low-temperature domains (near the glass transition temperature range – cf. Table 4 and Figure 3), the viscosity of these materials depends on the Ce addition and Ce oxidation state (cf. Table 5, Figure 3). For instance, for silicates containing other

multivalent elements (e.g., Fe^{2+}, Fe^{3+}), viscosity changes are more pronounced at relatively low-temperature domains because entropic effects due to chemical mixing of elements and structural disorder become more relevant, making viscosity more sensitive to chemical and structural changes.[25, 53] For depolymerized melts, such as the studied case, a small change in composition and structure generally causes an insignificant change in viscosity at relatively high-temperature regions, as observed here.[25, 53]

In terms of the effect of Ce addition on the viscosity of these materials, Müller et al.[22] and Müller & Dingwell[54] recently studied the viscosity of molten glasses containing different lanthanides, including Ce. It has been observed that upon Ce addition, there is a slight decrease in viscosity at high-temperature domains and a relatively strong increase in viscosity at low-temperature ranges. Here, we observe that around the glass transition temperature range, the same behavior occurs, but with lower intensity. This difference may be attributed to the different amounts of Ce between the different studies. While our glasses contain ~1.3 mol%, Müller et al. added ~5.3 mol% to their Na-disilicate base composition. We chose this amount of Ce due to the different solubilities of trivalent and tetravalent Ce ions in silicate melts, aiming to enhance the studied redox range.[36] Therefore, the effect observed in their study is more pronounced but, overall, both studies exhibit the same trend at low temperature range. Similarly, Cicconi et al.[11] observed that the addition of Ce in silicate systems induced an increase in T_g values and, consequently, in viscosity values at low-temperature regions. Consistent with these findings, Mekki[12] also showed that the addition of Ce in sodium silicate glasses leads to an increase of glass transition temperatures. The increase in T_g observed by Mekki is almost linear with an increase of about 15 °C with addition of 2.5 mol% CeO_2. This value is very similar to the 17 °C increase in T_g we report in Table 4 with addition of 1.3 mol% Ce_2O_3 (2.6 mol% CeO_2).

In terms of the effect of Ce reduction on the viscosity of these glasses and melts, Cicconi et al.[11] studied Ce-bearing glasses and determined their glass transition temperatures as a function of Ce redox state. Similar to the current study, they observed an augmentation in the glass transition temperatures of Ce-bearing glasses upon Ce reduction. Müller et al.[22] and Müller & Dingwell[54] presented data on lanthanide-bearing silicate glasses (NS2 and CMAS, respectively), while their Ce-bearing compositions showed lower viscosity values than the overall trend shown by their counterparts at high temperature regimes. In these studies, it has been claimed that this viscosity decreasing effect might be related to the multivalent speciation of Ce in the melt (both, Ce^{3+} and Ce^{4+} are potentially present) while the other lanthanides (except Eu) present a valence of +3 in the investigated silicate glasses. For the low temperature regime, the current study supports the findings of Müller et al.[22], as the relative proportion of Ce^{4+} increases (going from condition c to condition a), viscosity decreases (Table 7). This confirms that the addition of Ce in the glass leads to a smaller increase in viscosity than the addition of a non-multivalent REE, and supports the hypothesis made by Müller et al. that this behavior is due to the partial oxidation of Ce^{3+} to Ce^{4+}.

In order to link the change in rheological properties to a structural change during Ce_2O_3 addition and reduction, we present in Figure 7 the relative area of each contribution highlighted in the Raman decomposition in section 3.3 and Figure 6. It is important to emphasize that we are not displaying the speciation (i.e., relative amount)

of the Q^n units, but rather the relative area related to each of these Q^n units. Figure 9 shows the changes in the relative area of each band upon Ce_2O_3 addition as well as for the Ce_2O_3 reduction in the glass. As previously noted, a $Q^{2(Ce)}$ band rises upon Ce_2O_3 addition, while the bands associated with $Q^{3(II)}$ and Q^4 species diminish, pointing to Ce_2O_3 decreasing the overall polymerization of the melt. At this stage of the discussion, we do not differentiate Ce^{3+} and Ce^{4+}, the overall depolymerization observed is therefore due to a mixture of both Ce^{3+} and Ce^{4+}. This depolymerization effect upon CeO_2 oxide addition has been previously observed in different systems.[55–57]. Notably, Fu et al.[58] studied the impact of Ce addition on the viscosity and structure of a borosilicate glass using Raman as well as ^{29}Si and ^{11}B NMR spectroscopies. They also evidenced depolymerization of the glass network upon Ce addition with the conversion of Q^4 units to Q^3 units and BO_4 to BO_3 units, even for low amounts of Ce. However, they showed that Ce-doping levels as low as 0.6 wt% CeO_2 can lead to a viscosity increase at high temperature, this observation has not been reproduced in our study nor in Muller & Dingwell's[54] where Ce addition was found to lower high temperature viscosity of a CMAS glass. This high viscosity increase, despite the depolymerization of the glass network is reminiscent to what we observed near T_g. Notably, Fu et al. studied borosilicate melts where Ce can be used by BO_4 as charge compensator rather than a network modifier. This could explain the increase in high temperature viscosity they report with Ce addition.

Structural and vibrational changes are caused not only by the addition of Ce to the glassy network but also by its redox state. Upon Ce reduction, the relative contribution of the $Q^{2(Ce)}$ band diminishes sharply, indicating that this contribution is mainly due to tetravalent Ce, and might be linked to the high field strength of this cation. However, under the most reducing conditions (i.e., sample named WG 1.3 Ce_2O_3 - c), the relative area of this band is not negligeable, meaning that trivalent Ce also contributes, albeit to a lesser degree. The $Q^{3(Ce)}$ band is also impacted, though to a lesser extent, suggesting that trivalent and tetravalent Ce have similar contributions to this $Q^{3(Ce)}$ vibration.

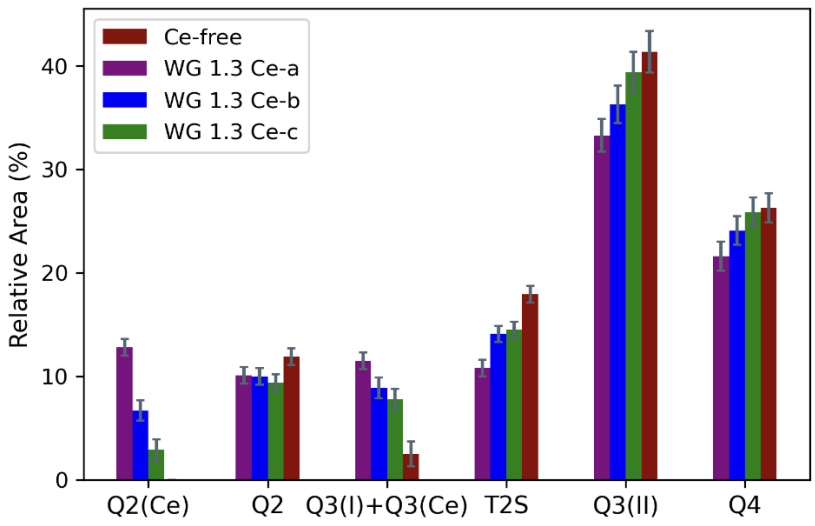

Figure 9: Relative areas of the bands obtained by decomposition for the Ce-free sample together with the Ce-bearing glasses for different redox conditions.

In order to distinguish the impact of trivalent and tetravalent Ce on the glass structure, it is worth focusing on the WG 1.3 Ce-c sample as XANES data confirm its full reduction. Therefore, any structural difference with the Ce-free glass is due to trivalent Ce. The decomposition of Raman spectra indicates that trivalent Ce favors the formation of $Q^{3(Ce)}$ species while marginally changing the overall glass polymerization. The main structural difference upon trivalent Ce addition is the apparition of a new type of Q^3 units.

However, in samples WG 1.3 Ce_2O_3-a and -b, Ce is partially oxidized to its tetravalent state (see XANES data in Table 7). As stated earlier, tetravalent Ce is the main contributor to the $Q^{2(Ce)}$ vibration, thus depolymerizing the melt structure. However, due to the high cationic field strength of Ce(IV), it is likely that these $Q^{2(Ce)}$ units lower viscosity less than regular Q^2 units. Upon Ce reduction, these $Q^{2(Ce)}$ units get converted to $Q^{3(Ce)}$, thereby increasing melt polymerization and viscosity.

Trivalent Ce possesses a higher cationic field strength (0.53 $Å^{-2}$) compared to Na (0.19 $Å^{-2}$), Ca (0.33 $Å^{-2}$) and Mg (0.46 $Å^{-2}$),[57] resulting in the NBO-Ce(III) bond being much more covalent and, consequently, stronger than those involving alkali/alkali-earth ions. Since the Si-O-Ce(III)-O-Si linkage is a strong one, the rise of $Q^{3(Ce)}$ units could explain the viscosity increase at relatively low temperatures upon trivalent Ce addition.

We can therefore conclude that Ce^{3+} and Ce^{4+} have different effect on the structure and viscosity of the studied silicate system. Ce^{3+} does not significantly change the polymerization of the glass but creates a relatively strong linkage between NBOs. This leads to an increase in glass transition temperature upon Ce^{3+} addition as shown between samples Ce-free and WG-1.3-Ce2O3-c (Table 6).

The oxidation of Ce^{3+} to Ce^{4+} leads to a depolymerization of the network and therefore a decrease of T_g relative to the fully reduced sample. When Ce is added to the glass, the reduced species leads to an increase in T_g while the oxidized one tends to decrease this characteristic temperature. In the case of this study, Ce^{3+} is the dominant specie and it leads to an overall increase in T_g despite the network being depolymerized.

Since at low temperatures the viscosities of these materials change upon Ce addition and reduction, and, on the other hand, at relatively high temperatures it remains constant, one can expect that these materials would have different fragilities. Thus, the Ce-bearing samples present a considerably higher deviation from the Arrhenian behavior when compared to the Ce-free samples, characterizing them by higher fragilities (cf. Table 5). Indeed, as we calculated, Ce-bearing glasses have considerably higher fragilities than the Ce-free sample. This behavior has been already reported in the literature for lanthanides-bearing glasses.[53] The observed changes in fragility in these glasses might have an impact on the processability of Ce-bearing glasses in industrial contexts. Indeed, the working range of a glass can be defined as the temperature interval were viscosity is between 10^2-10^3 to $10^{6.6}$ Pa.s[59, 60] (called the workability region). An increase in fragility implies that viscosity is more sensitive to temperature changes,[59] which leads to the working range being smaller when forming the glass. From an industrial standpoint, it means that when melt fragility increases, the forming of

the glass needs to happen in a narrower window of temperature. As Ce_2O_3 addition increases melt fragility it diminishes the working range making glass forming more difficult.

5. CONCLUSIONS

We studied the viscosity of Ce-free and Ce-bearing window glasses containing ~1.3 mol% of Ce_2O_3 (i.e., ~6.5 wt.%) at both relatively high- and low-temperature domains, equilibrated with gas mixtures to achieve different redox conditions. We demonstrate that the viscosities of these systems do not significantly change at relatively high-temperature domains (i.e., ~1200 °C) for both Ce addition and reduction. This observation implies that Ce_2O_3 addition of 1.3 mol% does not change the melt viscosity once the bubbles induced by the fining process have left the melt. This is of particular interest in industrial contexts where Ce oxide is widely used as fining agent. However, at low temperature domains, close to the glass transition temperature at ca. 600 °C, we observe a slight increase in viscosity upon Ce addition and Ce reduction. Importantly, we ruled out the remaining silicate composition as the cause of the observed viscosity changes, establishing that Ce itself was the primary factor influencing the viscosity behavior. We supported these findings using XANES spectroscopy to confirm the reduction of Ce obtained using the gas mixtures. In addition, Raman spectroscopic results allowed us to describe the polymerization behavior during Ce addition and reduction processes.

ACKNOWLEDGMENTS

Adrien Donatini acknowledges support of the ANRT and Corning SAS under the CIFRE Contract 2021/0986. Luiz Pereira is grateful for the support of the Alexander von Humboldt Foundation. Luiz Pereira also thanks the staff of Altunizade, Nuhkuyusu Cd No:94, 34662 Üsküdar, İstanbul, Türkiye for the support during the preparation of the manuscript. We acknowledge support of the European Research Council (ERC) 2018 ADV Grant 834225 (EAVESDROP). The authors thank SOLEIL (Saint-Aubin, France) for provision of synchrotron radiation facilities (project number 20221616). We also thank Alexander Pitsch and Anatoly Arkhipin for lending us part of their beamline time as well as Nicolas Trcera for the assistance in using beamline LUCIA.

REFERENCES

1. Cicconi MR, Le Losq C, Henderson GS, Neuville DR. The Redox Behavior of Rare Earth Elements. 1st ed. In: Moretti R, Neuville DR, eds. *Geophysical Monograph Series*, 1st ed. Wiley; 2021:381–398. https://doi.org/10.1002/9781119473206.ch19
2. Tanabe S. Glass and Rare-Earth Elements: A Personal Perspective. *International Journal of Applied Glass Science*. 2015;6(4):305–328. https://doi.org/10.1111/ijag.12142
3. Moretti R. Polymerisation, basicity, oxidation state and their role in ionic modelling of silicate melts. *Annals of Geophysics*. 2005;48(4–5). https://doi.org/10.4401/ag-3221
4. Kress VC, Carmichael ISE. The compressibility of silicate liquids containing Fe_2O_3 and the effect of composition, temperature, oxygen fugacity and pressure on their redox states. *Contributions to Mineralogy and Petrology*. n.d.;108:82–92.
5. Pinet O, Phalippou J, Di Nardo C. Modeling the redox equilibrium of the Ce^{4+}/Ce^{3+} couple in silicate glass by voltammetry. *Journal of Non-Crystalline Solids*. 2006;352(50–51):5382–5390. https://doi.org/10.1016/j.jnoncrysol.2006.08.034

6. Herrmann A, Othman HA, Assadi AA, Tiegel M, Kuhn S, Rüssel C. Spectroscopic properties of cerium-doped aluminosilicate glasses. *Opt Mater Express, OME*. 2015;5(4):720–732. https://doi.org/10.1364/OME.5.000720
7. Gin S, Jollivet P, Tribet M, Peuget S, Schuller S. Radionuclides containment in nuclear glasses: an overview. *Radiochimica Acta*. 2017;105(11):927–959. https://doi.org/10.1515/ract-2016-2658
8. Pigeonneau F, Pereira L, Laplace A. Dynamics of rising bubble population undergoing mass transfer and coalescence in highly viscous liquid. *Chemical Engineering Journal*. 2023;455:140920. https://doi.org/10.1016/j.cej.2022.140920
9. Pereira L, Kloužek J, Vernerová M, Laplace A, Pigeonneau F. Experimental and numerical investigations of an oxygen single-bubble shrinkage in a borosilicate glass-forming liquid doped with cerium oxide. *J Am Ceram Soc*. 2020;103(12):6736–6745. https://doi.org/10.1111/jace.17398
10. Pereira L, Neyret M, Laplace A, Pigeonneau F, Nuernberg R. Inferring bubble volume fraction in a glass melt through in situ impedance spectroscopy measurements. *International Journal of Applied Glass Science*. 2021;12(3):358–366. https://doi.org/10.1111/ijag.15895
11. Cicconi MR, Veber A, Neuville D, Baudelet F, De Ligny D. Cerium speciation in silicate glasses: Structure-property relationships. *Journal of Non-Crystalline Solids*. 2021;563:120785. https://doi.org/10.1016/j.jnoncrysol.2021.120785
12. Mekki A. X-ray photoelectron spectroscopy of CeO_2–Na_2O–SiO_2 glasses. *Journal of Electron Spectroscopy and Related Phenomena*. 2005;142(1):75–81. https://doi.org/10.1016/j.elspec.2004.09.001
13. Pereira L, Podda O, Fayard B, Laplace A, Pigeonneau F. Experimental study of bubble formation in a glass-forming liquid doped with cerium oxide. *Journal of the American Ceramic Society*. 2020;103(4):2453–2462. https://doi.org/10.1111/jace.16950
14. Pereira L, Vasseur J, Wadsworth FB, Trixler F, Dingwell DB. Interparticle and Brownian forces controlling particle aggregation and rheology of silicate melts containing platinum-group element particles. *Sci Rep*. 2022;12(1):9226. https://doi.org/10.1038/s41598-022-12948-1
15. Cassar DR, Rodrigues AM, Nascimento MLF, Zanotto ED. The diffusion coefficient controlling crystal growth in a silicate glass-former. *Int J of Appl Glass Sci*. 2018;9(3):373–382. https://doi.org/10.1111/ijag.12319
16. Pigeonneau F. Mass transfer of a rising bubble in molten glass with instantaneous oxidation–reduction reaction. *Chemical Engineering Science*. 2009;64(13):3120–3129. https://doi.org/10.1016/j.ces.2009.03.045
17. Dingwell D, Virgo D. The effect of oxidation state on the viscosity of melts in the system Na20-FeO-Fe203-Si02. *Geochimica et Cosmochimica Acta*. 1987;51:195–205.
18. Dingwell B, Virgo D. Viscosities of melts in the Na_2O-FeO-Fe_2O_3-SiO_2 system and factors controlling relative viscosities of fully polymerized silicate melts. *Geochimica et Cosmochimica Acta.* 1988; 52:395:403.
19. Dingwell D. Redox viscometry of some Fe-bearing silicate melts. *American Mineralogist*. 1991;76:1560–1562.
20. Casas AS, Hess K-U, Badro J, Eitel M, Dingwell DB. A redox effect on the viscosity of molten pyrolite. *Chemical Geology*. 2023;642:121816. https://doi.org/10.1016/j.chemgeo.2023.121816
21. Guo W, Wang Z, Zhao Z, An Z, Wang W. Effect of CeO_2 on the viscosity and structure of high-temperature melt of the CaO-SiO_2(-Al_2O_3)-CeO_2 system. *Journal of Non-Crystalline Solids*. 2020;540:120085. https://doi.org/10.1016/j.jnoncrysol.2020.120085
22. Müller D, Pereira L, Hess K-U, Dingwell DB. Influence of lanthanides on the melt viscosity and glass density of sodium disilicate. *Journal of Non-Crystalline Solids*. 2023;619:122565. https://doi.org/10.1016/j.jnoncrysol.2023.122565
23. Kirichenko AS, Nekhamin SM. Effect of Cerium Oxide on Acid Slag Viscosity. *Metallurgist*. 2020;64(5–6):548–552. https://doi.org/10.1007/s11015-020-01026-4
24. Wadsworth FB, Vasseur J, von Aulock FW, *et al.* Nonisothermal viscous sintering of volcanic ash. *Journal of Geophysical Research: Solid Earth*. 2014;119(12):8792–8804. https://doi.org/10.1002/2014JB011453
25. Chevrel MO, Giordano D, Potuzak M, Courtial P, Dingwell DB. Physical properties of $CaAl_2Si_2O_8$–$CaMgSi_2O_6$–FeO–Fe_2O_3 melts: Analogues for extra-terrestrial basalt. *Chemical Geology*. 2013;346:93–105. https://doi.org/10.1016/j.chemgeo.2012.09.004
26. Scherer GW. Use of the Adam-Gibbs Equation in the Analysis of Structural Relaxation. *Journal of*

the American Ceramic Society. 1984;67(7):504–511. https://doi.org/10.1111/j.1151-2916.1984.tb19643.x
27. Gottsmann J, Giordano D, Dingwell DB. Predicting shear viscosity during volcanic processes at the glass transition: a calorimetric calibration. *Earth and Planetary Science Letters*. 2002;198(3–4):417–427. https://doi.org/10.1016/S0012-821X(02)00522-8
28. Vantelon D, Trcera N, Roy D, *et al.* The LUCIA beamline at SOLEIL. *J Synchrotron Rad*. 2016;23(2):635–640. https://doi.org/10.1107/S1600577516000746
29. Newville M. Larch: An Analysis Package for XAFS and Related Spectroscopies. *J Phys: Conf Ser*. 2013;430:012007. https://doi.org/10.1088/1742-6596/430/1/012007
30. Wojdyr M. Fityk: a general-purpose peak fitting program. *J Appl Cryst*. 2010;43(5):1126–1128. https://doi.org/10.1107/S0021889810030499
31. Fulcher GS. ANALYSIS OF RECENT MEASUREMENTS OF THE VISCOSITY OF GLASSES. *J American Ceramic Society*. 1925;8(6):339–355. https://doi.org/10.1111/j.1151-2916.1925.tb16731.x
32. Tammann G, Hesse W. Die Abhängigkeit der Viscosität von der Temperatur bie unterkühlten Flüssigkeiten. *Z Anorg Allg Chem*. 1926;156(1):245–257. https://doi.org/10.1002/zaac.19261560121
33. Vogel H. Das Temperaturabhaengigkeitsgesetz der Viskositaet von Fluessigkeiten. *Physikalische Zeitschrift*. 1921;22:645.
34. Angell CA. Relaxation in liquids, polymers and plastic crystals — strong/fragile patterns and problems. *Journal of Non-Crystalline Solids*. 1991;131–133:13–31. https://doi.org/10.1016/0022-3093(91)90266-9
35. Burnham AD, Berry AJ. The effect of oxygen fugacity, melt composition, temperature and pressure on the oxidation state of cerium in silicate melts. *Chemical Geology*. 2014;366:52–60. https://doi.org/10.1016/j.chemgeo.2013.12.015
36. Cachia J-N, Deschanels X, Den Auwer C, *et al.* Enhancing cerium and plutonium solubility by reduction in borosilicate glass. *Journal of Nuclear Materials*. 2006;352(1–3):182–189. https://doi.org/10.1016/j.jnucmat.2006.02.052
37. Donatini A, Georges P, Fevre T, Cormier L, Neuville DR. Investigating cerium redox changes between aluminosilicate glass and melt: A multispectroscopic approach. *The Journal of Chemical Physics*. 2024;160:124503.
38. Yadav AK, Singh P. A review of the structures of oxide glasses by Raman spectroscopy. *RSC Adv*. 2015;5(83):67583–67609. https://doi.org/10.1039/C5RA13043C
39. Virgo D, Mysen BO, Kushiro I. Anionic Constitution of 1-Atmosphere Silicate Melts: Implications for the Structure of Igneous Melts. *Science*. 1980;208(4450):1371–1373. https://doi.org/10.1126/science.208.4450.1371
40. Kalampounias AG. IR and Raman spectroscopic studies of sol–gel derived alkaline-earth silicate glasses. *Bull Mater Sci*. 2011;34(2):299–303. https://doi.org/10.1007/s12034-011-0064-x
41. McMillan P. Structural studies of silicate glasses and melts-applications and limitations of Raman spectroscopy. *American Mineralogist*. 1984;69:622–644.
42. Trcera N, Rossano S, Tarrida M. Structural study of Mg-bearing sodosilicate glasses by Raman spectroscopy: Structure of Mg-bearing glasses. *J Raman Spectrosc*. 2011;42(4):765–772. https://doi.org/10.1002/jrs.2763
43. Shannon RD. Revised effective ionic radii and systematic studies of interatomic distances in halides and chalcogenides. *Acta Crystallographica Section A*. 1976;32(5):751–767. https://doi.org/10.1107/S0567739476001551
44. Le Losq C, Neuville DR. Effect of the Na/K mixing on the structure and the rheology of tectosilicate silica-rich melts. *Chemical Geology*. 2013;346:57–71. https://doi.org/10.1016/j.chemgeo.2012.09.009
45. Neuville DR. Viscosity, structure and mixing in (Ca, Na) silicate melts. *Chemical Geology*. 2006;229(1–3):28–41. https://doi.org/10.1016/j.chemgeo.2006.01.008
46. Schaller T, Stebbins JF, Wilding MC. Cation clustering and formation of free oxide ions in sodium and potassium lanthanum silicate glasses: nuclear magnetic resonance and Raman spectroscopic findings. *Journal of Non Crystalline Solids*. 1999;243:146–157.
47. Ellison AJG, Hess PC. Lanthanides in silicate glasses: A vibrational spectroscopic study. *Journal of Geophysical Research: Solid Earth*. 1990;95(B10):15717–15726. https://doi.org/10.1029/JB095iB10p15717
48. Cassar DR. GlassNet: A multitask deep neural network for predicting many glass properties. *Ceramics International*. 2023;49(22):36013–36024. https://doi.org/10.1016/j.ceramint.2023.08.281
49. Duan X. A model for calculating the viscosity of natural iron-bearing silicate melts over a wide range

of temperatures, pressures, oxygen fugacites, and compositions. *American Mineralogist*. 2014;99(11–12):2378–2388. https://doi.org/10.2138/am-2014-4841
50. Hui H, Zhang Y. Toward a general viscosity equation for natural anhydrous and hydrous silicate melts. *Geochimica et Cosmochimica Acta*. 2007;71(2):403–416. https://doi.org/10.1016/j.gca.2006.09.003
51. Giordano D, Russell JK, Dingwell DB. Viscosity of magmatic liquids: A model. *Earth and Planetary Science Letters*. 2008;271(1–4):123–134. https://doi.org/10.1016/j.epsl.2008.03.038
52. Langhammer D, Di Genova D, Steinle-Neumann G. Modeling Viscosity of Volcanic Melts With Artificial Neural Networks. *Geochem Geophys Geosyst*. 2022;23(12):e2022GC010673. https://doi.org/10.1029/2022GC010673
53. Le Losq C, Cicconi MR, Neuville DR. Iron in Silicate Glasses and Melts. *Magma Redox Geochemistry*. American Geophysical Union (AGU); 2021:233–253. https://doi.org/10.1002/9781119473206.ch12
54. Müller D, Dingwell DB. Calcium–magnesium–aluminum-silicate melt viscosities influenced by lanthanides, yttrium, and zirconium. *Journal of the American Ceramic Society*. 2024;107(5):2785–2792. https://doi.org/10.1111/jace.19646
55. Qi J, Liu C, Zhang C, Jiang M. Effect of Ce2O3 on Structure, Viscosity, and Crystalline Phase of CaO-Al_2O_3-Li_2O-Ce_2O_3 Slags. *Metall Mater Trans B*. 2017;48(1):11–16. https://doi.org/10.1007/s11663-016-0850-3
56. Aboelwafa MA, Meikhail MS, Oraby AH, Abdelghany AM. Influence of Cerium oxide on the structural aspects of soda-lime aluminosilicate glasses synthesized by sol-gel route. *Materials Chemistry and Physics*. 2023;305:127930. https://doi.org/10.1016/j.matchemphys.2023.127930
57. Ellison AJG, Hess PC. Vibrational spectra of high-silica glasses of the system K20-SiO2-La203. *Journal of Non Crystalline Solids*. 1991;127:247–258.
58. Fu J, Zhao J, Li S, *et al.* Influence of CeO_2 on the structure and properties of borosilicate glass: An investigation from the perspective besides the refining process. *Journal of Non-Crystalline Solids*. 2024;623:122690. https://doi.org/10.1016/j.jnoncrysol.2023.122690
59. Hrma P, Ferkl P, Kruger AA. Glass length: Workability and meltability of glass as a function of glass melt fragility. *Journal of Non-Crystalline Solids*. 2022;597:121931. https://doi.org/10.1016/j.jnoncrysol.2022.121931
60. Wang M, Fang L, Li M, *et al.* Dependence of Gd_2O_3 containing silicate glass workability and fragility on structure. *Materials Chemistry and Physics*. 2016;179:304–309. https://doi.org/10.1016/j.matchemphys.2016.05.043